Design Studies for the Proposed CESR Accelerator Test Facility

A THESIS SUBMITTED TO THE UNDERGRADUATE PROGRAM OF THE INSTITUTE OF TECHNOLOGY OF THE UNIVERSITY OF MINNESOTA BY

Michael Paul Ehrlichman

IN PARTIAL FULFILLMENT OF THE REQUIREMENTS FOR THE DEGREE OF BACHELOR OF SCIENCE WITH LATIN HONORS

Acknowledgments

I would like to thank Mark Palmer of Cornell University for mentoring me in accelerator physics and proofreading this thesis, and Dave Sagan also of Cornell University for providing invaluable advice regarding mathematics and computer programming. I would like to thank Ron Poling of the University of Minnesota and Maury Tigner of Cornell University for providing me with research opportunities in accelerator physics. I would like to thank Ron Poling for providing me with advice throughout my undergraduate education and for proofreading this thesis. I would like to thank David Rubin of Cornell University for helping me understand the BMADZ optimizer and taking the time to write up memos explaining some of the more difficult accelerator concepts.

Abstract. This thesis describes research undertaken in collaboration with accelerator physicists at Cornell University to develop and test designs and simulation tools for the CESR Test Accelerator (CesrTA) and International Linear Collider (ILC). Specifications for the ILC call for ultra-low emittance beams in order to meet luminosity requirements. Phenomena such as electron cloud effects and ion instabilities that are secondary in currently running accelerators, have the potential to significantly impact the performance of the ILC. The behavior of these phenomena and methods for mitigating them need to be explored to ensure the the ILC is correctly designed. CESR is a 768 meter electron-positron storage ring that employs technology similar to that which will be used in the ILC. It has been proposed that CESR be reconfigured for low-emittance operation at energies ranging from 1.5 GeV to 5.0 GeV and used as a test bed for the ILC. We find that CesrTA has the potential to produce beams with vertical emittances less than 10 pm and Touschek lifetimes ranging from 30 minutes to several hours when intrabeam scattering effects are taken into account.

I. INTRODUCTION

The next accelerator planned to work at the frontier of high energy physics, the role that will be held beginning in 2008 by CERN's Large Hadron Collider, is the International Linear Collider (ILC). The ILC will be an electron-positron collider with two opposing linacs generating very dense beams with energies ranging from 0.25 to 0.5 TeV. The fundamental nature of the electron/positron collisions will give precise measurements of the particles discovered with the LHC. These measurements will almost certainly impact how the standard model is viewed - by confirming or denying the existence of the Higgs - and hopefully by telling us which of the newer models, such as minimally symmetric super symmetry and extra-dimensions, gives the best agreement with experiment.

New physical discoveries have typically been associated with higher energies. Higher energy accelerators create particles that lower energy accelerators cannot. A complementary approach to scientific discovery is that of high precision. Smaller error bars on empirical parameters can have drastic effects on the theoretical landscape. Hints at new physics beyond the standard model can lay in anomalies that are only discernible with high precision measurements.

The main reason electrons are better than protons for making high precision measurements is that they are fundamental particles. Every electron and every inelastic collision is (ignoring relative spin) identical. It is always known what particles went into the interaction, and their momenta are known to great precision. Protons, on the other hand, are not fundamental particles. They are composed of three quarks, two up and one down. In high-energy collisions, it is the quarks that interact. There are thus three possibilities in every proton-proton interaction, uu, ud, or dd. It is also unknown exactly how much momentum each of the interacting quarks has. Quarks rattle around inside the proton, and the distribution of the momentum among the three quarks is constantly changing. While the application of good statistical analysis techniques can minimize the uncertainty due to the non-fundamental nature of protons, the precision ultimately obtained is much worse than that which could be obtained with electrons. Note that actual high energy experiments can be set up to collide any pairwise combination of electrons, positrons, protons, and antiprotons. These same arguments can be extended to those cases.

Hadrons receive so much attention at the forefront of high-energy physics because they are heavier, and can therefore be accelerated to higher energies without the technological difficulties encountered at high relativistic gamma. The simple relation $\gamma = E/m_0$ (the convention of setting $c \equiv 1$ is applied throughout this thesis), tells us that electrons, which are 1800 times lighter than protons, have a γ 1800 times larger for a given energy. Maxwell's equations tell us that whenever a charged particle is accelerated, it radiates energy, and steering a particle means accelerating it. Protons and electrons are charged particles, and so when we try to steer them one way or another, they radiate energy. Our concern here is mainly with steering relativistic particles in a ring. The radiation given off as the particles are steered around a ring is called synchrotron radiation. A simple derivation gives the power radiated in the relativistic limit as

$$P_\gamma = \frac{1}{6\pi\epsilon_0}\frac{e^2 c}{\rho^2}\gamma^4 = \frac{1}{6\pi\epsilon_0}\frac{e^2 c}{\rho^2}\left(\frac{E}{m_0}\right)^4. \tag{1}$$

Recalling that an electron has about 1/1800 the mass of a proton, we see that, all else being equal, an electron at a particular energy will radiate $\sim 1800^4$ times as much power as a

proton! Maintaining the energy of a high energy electron traveling in a ring requires that a very large amount of energy be continually pumped back into the beam.

Because protons are heavier, they radiate away less of their energy when steered around a ring, and so are easier to accelerate to high energies. Protons can simply be run over and over again in a circle with a moderate per-turn acceleration gradient. This allows us to construct proton accelerators with such impressive energies as the Tevatron (1 TeV) and LHC (14 TeV). Synchrotron radiation can be mitigated by increasing the diameter of the ring (notice the $1/\rho^2$ dependence in equation 1). However, to reach energies with electron machines that approach those of proton machines, the radius would need to be over 16 times larger than the proton machine to stay within practical engineering limits.

The limits imposed by synchrotron radiation require that a high-energy electron collider be linear. In a linear collider, two opposing beams of particles are accelerated in opposite directions and collided in the middle.

Electrons have another advantage in that all of the beam energy goes into every collision. Due to their composite nature, when protons collide only about one-third of their energy goes into the collision. Studies indicate that a 500 GeV linear electron-positron collider (1 TeV CMS energy) would overlap the range of the 14 TeV LHC for statistically significant discovery.

The foregoing considerations tell us about the next high energy collider we need to build. It is known that high precision measurements at energies ranging from 0.25+0.25 TeV to 0.5+0.5 TeV will be needed to refine the results from the LHC. Current plans call initially for 0.25+0.25 TeV with 0.5+0.5 TeV upgrade capability. High precision measurements require the use of fundamental particles, electrons. Such a machine will need to be linear to avoid prohibitive synchrotron radiation losses. Since the machine will be linear, all the acceleration will need to be done in one pass. The limiting factor becomes the accelerating gradient - how much distance is necessary to accelerate an electron to 250 GeV? A fundamental relation, $E = V \times e$, tells us that a particle of charge e gains energy E when accelerated through a voltage potential V. Dividing the desired energy of 250 GeV by the charge of an electron, 1.6×10^{-19} Coulombs, gives a required potential of 2.5×10^{11} volts. The best practical option available today for accelerating structures is the superconducting radio-frequency cavity (SRF). Voltage gradients of 50 MV/m have been achieved with SRF cavities in the laboratory. For practical purposes, it is assumed that 35 MV/m cavities can be mass-produced and implemented in the ILC. Dividing the required potential (2.5×10^{11} volts) by the expected gradient (35 MV/m) gives a length of 7.5 km. Additional infrastructure increases this to 11 km. Since we are colliding opposing beams, we need to point two linacs at each other, doubling the length to 22 km. This is the proposed length of the ILC.

A schematic showing the major sections of the ILC is in figure 1. The steps involved in the production and acceleration of the electron and positron beams are as follows. First, electrons given off by a cathode are bunched and pre-accelerated to 5 GeV. These 5 GeV electrons are fed into the electron damping ring where their phase-space dimensions are shrunk. The damped electron bunches are injected into the main electron linac, where they are accelerated to the final collision energy. About half-way down the linac, the electrons travel through an undulator, which wiggles the electron to induce the production of γ-rays. The γ-rays are directed at a titanium alloy target to produce positrons. The positrons are then sent through a 5 GeV pre-accelerator, positron damping ring, and accelerated to the final beam energy and collided with the electrons.

Obtaining the desired energy is only half the story. Once we are at an energy capable

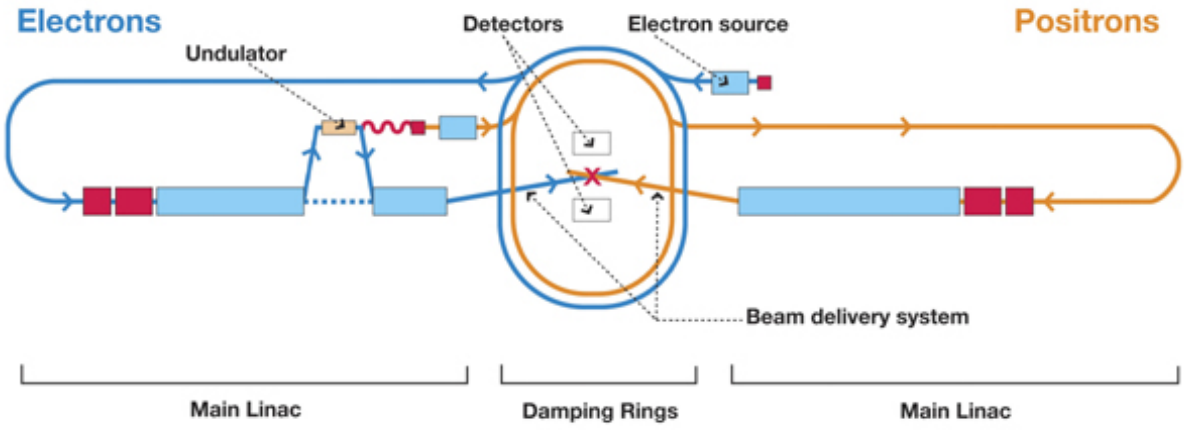

FIG. 1: Schematic of the ILC (not to scale), showing production, damping, and acceleration stages. Taken from the ILC Reference Design Report [1]

of producing particles of interest, we want to produce as many of them as possible. The analysis of high-energy physics data is a statistical process, governed by the fundamental relation that the uncertainty in measurements goes as $1/\sqrt{N}$, where N is the number of events. The rate at which a collider produces events is governed by a quantity called the luminosity. The luminosity is the interaction probability over time. Each event, for example the production of a Higgs boson, has a cross-section. The rate of a particular event is given by the luminosity multiplied by the cross-section of the event.

Luminosity is governed by the density of the bunches that make up the beam and the rate at which they collide. We want the luminosity to be as large as possible. It is given by

$$\mathcal{L} = \frac{1}{4\pi} \frac{f_{rep} N_1 N_2}{\sqrt{\beta_x \epsilon_x} \sqrt{\beta_y \epsilon_y}}, \tag{2}$$

where f_{rep} is how often bunches collide, $N_{1,2}$ is the number of particles in each bunch, and $\beta_{x,y}$ and $\epsilon_{x,y}$ quantify the size of the beam. The rate at which bunches collide is determined by how quickly the machine can generate electrons and positrons, process them into bunches, and accelerate them to the desired energy. This will range from 6.6 to 25.6 kHz for the ILC. The number of particles in each bunch is limited by instabilities that develop if the bunch charge is too high. $\beta_{x,y}$ at the IP is a measure of how strong the final focusing magnets are; more powerful magnets produce a smaller $\beta_{x,y}$ and squeeze the bunches to smaller dimensions before they collide. The smallness of $\beta_{x,y}$ is limited by superconducting magnet technology. Emittance $\epsilon_{x,y}$ is the area a bunch encloses in phase space. As a particle makes it way through an accelerator, it has a non-zero transverse motion, called betatron oscillations. At the peaks of these oscillations, the particle has zero transverse momentum, but is displaced far from the ideal path. At the nodes the particle intersects the ideal path, but has a high transverse momentum. Only bunches with a small phase-space area can ultimately be squeezed down to smaller dimensions at the interaction point. The parts of the ILC responsible for reducing the emittance of the beams are the damping rings.

Ignoring non-adiabatic effects, emittance is a conserved quantity. No combination of magnets of any number of poles or radio-frequency cavities can change the emittance of

a bunch of particles. But thankfully there are phenomena which move energy in or out of a bunch that can be exploited to alter a particle's emittance. In particular, synchrotron radiation can be used to remove transverse emittance. The same effect that limits our ability to build high energy electron rings, allows us to shrink the dimensions of electron bunches by several orders of magnitude. The power radiated by accelerating a charged particle is in the form of a photon. This photon is emitted perpendicular to the direction of the acceleration. For an electron traveling in a perfect circle, the emitted photon is tangent to the circle. Note that due to quantum mechanical effects there is a small uncertainty in the actual direction the photon is emitted. However, for present purposes this uncertainty is overshadowed by other effects and can be ignored. A photon emitted tangent to the circle is parallel to the electron's path, and so the momentum it carries away is longitudinal momentum - it slows the particle down. This energy is pumped back into the particle once it hits the RF cavities. Now imagine a bunch of particles with non-zero emittance such that many of the particles are undergoing betatron oscillations (see figure 2). The photons emitted by the oscillating particles will not be tangent to the circle, but parallel to the electrons' instantaneous velocity. The photons will carry away not only longitudinal momentum, but also some transverse momentum. This loss of transverse momentum reduces the emittance of the bunch. The longitudinal momentum is restored by the RF cavities, and so the end result is a bunch with the same energy and lower emittance. This process is called radiation damping.

FIG. 2: Process of radiation damping. A photon is emitted by the particle carrying away transverse and longitudinal momentum. The longitudinal momentum is added back to the particle by the RF-cavities. Vector addition gives a new, lower emittance.

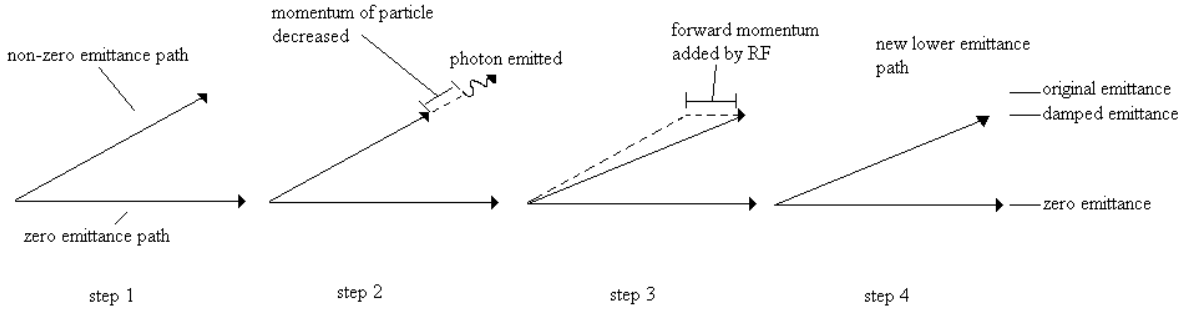

A way to enhance radiation damping in an accelerator is to use wigglers, shown in figure 3. A wiggler is a series of dipole magnets of alternating field gradient. When a beam passes through a wiggler, it undergoes a series of sharp bends that induce radiation damping.

The ILC damping rings will consist of a series of arcs and wigglers that reduce the emittance of 5 GeV beams received from the injectors to 2 pm before they are sent to the main linac. Emittance will, more or less, be conserved through the main linac, and so the emittance of the bunches at the crossing point will be that which can be achieved by the damping rings. Designing the damping rings to achieve these small emittances requires that the features of SRF-based wiggler-dominated electron rings be carefully studied.

The Cornell Electron Storage Ring (CESR) is a 768 meter circumference wiggler-dominated storage ring that uses radio-frequency cavities similar to those likely to be used for the ILC. It has been proposed that CESR be commissioned as a test accelerator for the ILC. Using CESR as an ILC test accelerator requires that it be reconfigured for low-

FIG. 3: Overhead and side views of wiggler and path taken by electron beam. The amplitude of the beam is exaggerated in this diagram, the actual amplitude is on the order of the beam dimensions. Photons are emitted throughout the wiggler, inducing radiation damping.

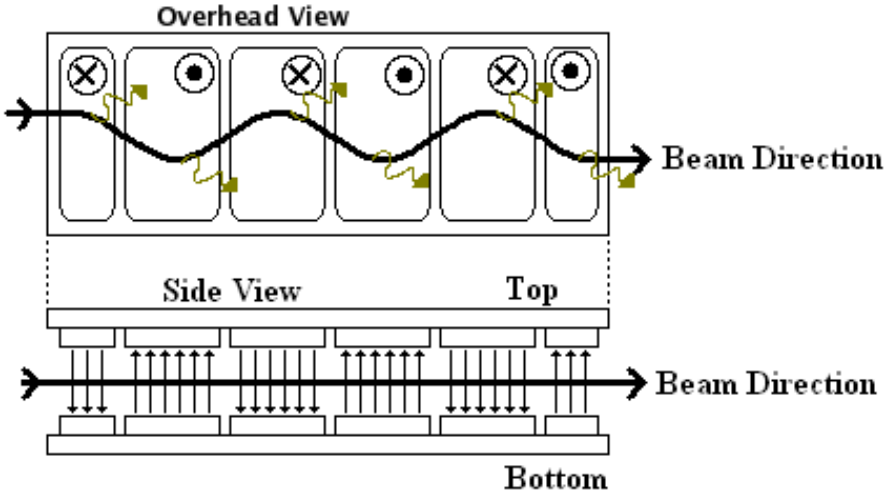

emittance operation. It needs to be able to generate low-emittance beams and store them for long enough periods of time to explore the properties of the beam.

My contributions to the CESR Test Accelerator consist of optimizing the optics functions of the lattice by optimizing the quadrupole and sextupole strengths around the ring, and determining the effects of intrabeam Coulomb scattering. Quadrupole optimization consists of minimizing the size of the beam through the wigglers to decrease its zero-current emittance. Sextupole optimization consists of correcting the chromaticity of the machine without destroying its dynamic aperture, thus ensuring non-problematic injection and a long beam lifetime. Intrabeam Coulomb scattering occurs when the bunches become dense enough so that pair-wise scattering events become significant. Scattering events that impart a large momentum deviation to the particles such that they are kicked out of the RF bucket are called Touschek losses and limit the lifetime of the beam. Lower momentum transfer events couple the beam dimensions and can blow up the emittance of the beam. In the sections that follow I will explain and discuss in detail the ideas mentioned here.

II. ACCELERATOR PHYSICS

In a storage ring, the beam is bent and focused using a system of multipole magnets. The system of multipole magnets creates a magnetic object called a guide field. To first order, the guild field is parameterized by four variables, β, α, γ, and η. The guide field can be thought of analogously to a slide with a rounded bottom such as might be found in a children's park. Imagine that you took a ball and threw it down the slide. The ball would make its way down the slide, undergoing oscillations according to the amount of transverse momentum you put into the ball. These oscillations are analogous to the betatron oscillations in an accelerator. The smaller the radius of curvature of the slide, the smaller the amplitude of the oscillations and the higher their frequency. The radius of curvature of the slide is analogous to the β function parameter of a magnetic guide field. In particular, a slide with a small radius of curvature corresponds to a strong quadrupole moment in the guide field. α is defined as

the derivative of beta with respect to the distance s along the beam path, $\alpha = -\frac{1}{2}\frac{d\beta}{ds}$ - how quickly the curvature of the slide changes as you move along it. γ is defined by $\frac{1+\alpha^2}{\beta}$, and μ is the phase advance per revolution, $\mu = 2\pi Q$, where Q is the number of betatron oscillations a particle makes per revolution.

A. Magnetic Lattice

The cyclotron equation tells us that to bend a particle of momentum p and charge e in a circle of radius R, a magnetic field of strength

$$B = \frac{p}{R \times e} \tag{3}$$

is required. Equation 3 can be rearranged to read

$$\frac{1}{R} = \frac{e}{p}B. \tag{4}$$

As the particles in a bunch travel around the lattice, they oscillate around the ideal orbit. The distance a particle is from the ideal orbit is x. Since $x << R$, we can expand the B field as a Taylor series,

$$B(x) = B_0 + \frac{dB}{dx}x + \frac{1}{2!}\frac{d^2B}{dx^2}x^2 + \frac{1}{3!}\frac{d^3B}{dx^3}x^3 + ... \tag{5}$$

Multiplying by e/p gives

$$\frac{e}{p}B(x) = \frac{e}{p}B_0 + \frac{e}{p}\frac{dB}{dx}x + \frac{e}{p}\frac{1}{2!}\frac{d^2B}{dx^2}x^2 + \frac{e}{p}\frac{1}{3!}\frac{d^3B}{dx^3}x^3 + ... \tag{6}$$

We see that the first term in equation 6 is simply the dipole in equation 4. Correspondingly, we can identify the rest of the terms in the expansion with multipoles,

$$\frac{e}{p}B(x) = \frac{1}{R} + kx + \frac{1}{2!}mx^2 + \frac{1}{3!}ox^3 + ..., \tag{7}$$

where $1/R$, k, m, and o correspond to multipole strengths. $1/R = B_z$ corresponds to the dipole and is used for steering. $k = \frac{e}{p}\frac{dB_z}{dx}$ corresponds to the quadrupole and is used for focusing. $m = \frac{1}{2!}\frac{e}{p}\frac{d^2B_z}{dx^2}$ corresponds to the sextupole and is used for chromaticity correction. $o = \frac{1}{3!}\frac{e}{p}\frac{d^3B_z}{dx^3}$ corresponds to an octopole and is used to control instabilities.

Table I gives the field distribution of the various multipoles, where x indicates the transverse displacement from the center of the magnet.

B. Linear Equations of Motion

To describe the motion of a particle around a storage ring, we attach a moving coordinate system K(x,z,s) to the ideal orbit a particle may take around a ring, figure 4.

TABLE I: Field distribution of multipole magnets as a function of distance from the magnet center. I_0 refers to the current in the magnet, a is the distance between the poles.

multipole	$B_z(x)$
dipole	$-\frac{\mu_0 I_0}{2a}$
quadrupole	$-\frac{\mu_0 I_0}{2a^2}\|x\|$
sextupole	$-\frac{\mu_0 I_0}{2a^3}\|x\|^2$

FIG. 4: The coordinate system $K = (x, z, s)$ moves around the ring attached to the nominal particle trajectory. K lays tangent to the ring, and z points perpendicular to the plane of the ring.

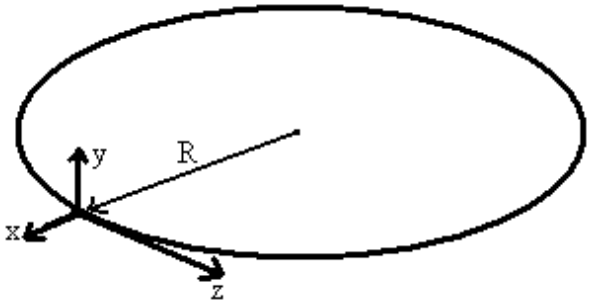

The z-coordinate of K is fixed to the tangent of the ideal orbit, and, assuming a flat orbit, the y-coordinate is perpendicular to the plane of the ring. Inside K the equations of motion of a particle traveling around a ring are

$$x''(s) + \left(\frac{1}{R^2(s)} - k(s)\right) = \frac{1}{R(s)}\frac{\delta p}{p}, \tag{8}$$

and

$$z''(s) + k(s)z(s) = 0, \tag{9}$$

where $\frac{\delta p}{p}$ refers to the momentum deviation of the particle. Particles of higher momentum take longer paths through the bends, and so are displaced transversely according to their momentum deviation. In straight regions, the radius of curvature, R, goes to infinity, and equations 8 and 9 differ only by the sign of k(s).

Most modern synchrotrons use separated function magnets. Separated function magnets have either a dipole field or a quadrupole field, but not both. The magnetic structure of such storage rings can be described as a series of bends, focusing elements, and drifts. This simplifies the the evaluation of equation 8 since we can assume that $R = \infty$ and/or $k = 0$. In a focusing element we assume $R \to \infty$, and equation 8 has the general solution

$$x(s) = \begin{cases} x_0 cosh\sqrt{k}s + \frac{x_0'}{\sqrt{k}} sinh\sqrt{k}s & k > 0 \text{ (defocusing)} \\ x_0 cos\sqrt{k}s + \frac{x_0'}{\sqrt{k}} sin\sqrt{k}s & k < 0 \text{ (focusing)}, \end{cases} \tag{10}$$

and

$$x'(s) = \begin{cases} x_0\sqrt{k} sinh\sqrt{k}s + x_0' cosh\sqrt{k}s & k > 0 \text{ (defocusing)} \\ x_0' cos\sqrt{k}s - \frac{x_0}{\sqrt{k}} sin\sqrt{k}s & k < 0 \text{ (focusing)}. \end{cases} \tag{11}$$

In a drift we assume $R = \infty$ and $k = 0$, and equation 8 has the solution

$$x(s) = x_0 + sx_0', \tag{12}$$

and

$$x'(s) = x'_0. \tag{13}$$

In a bend, $R < \infty$, and the forcing term in equation 8 does not vanish. It is useful to consider the case where $\delta p/p = 1$, and we define the dispersion function $D(s)$ as

$$D''(s) + \frac{1}{R^2}D(s) = \frac{1}{R}. \tag{14}$$

Note that we have also assumed that R is constant, which reflects that synchrotrons typically employ dipoles with a constant field. The general solution for equation 14 is

$$D(x) = D_0 cos\frac{s}{R} + D'_0 R sin\frac{s}{R} + R(1 - cos\frac{s}{R}), \tag{15}$$

$$D'(s) = -\frac{D_0}{R}sin\frac{s}{R} + D'_0 cos\frac{s}{R} + sin\frac{s}{R}. \tag{16}$$

With the dispersion function thus defined, we can write the orbit a particle takes as

$$x_g(s) = x(s) + D(s)\frac{\delta p}{p}. \tag{17}$$

C. Equilibrium beam emittance

In a wiggler dominated storage ring the equilibrium beam emittance is determined by competition between radiation damping and photon emission in dispersive regions.

When a photon is emitted in a dispersive region, the particle takes on a small momentum deviation, $\delta p/p$. Observing equation 17, we see that changing the momentum deviation of a particle in a region where $D(s) \neq 0$ changes the closed orbit of the particle. The particle then begins oscillating around the new closed orbit from a position that corresponded to its old closed orbit, resulting in larger amplitude oscillations.

In a damping ring, the wigglers are placed in regions where the dispersion is zero. The wigglers then have solely a damping effect on the beam, and the entire emittance contribution comes from photon emission in the bends. The general expression for the emittance of an electron beam in a lattice consisting entirely of bends is

$$\epsilon_x = \frac{55}{32\sqrt{3}}\frac{\hbar}{mc}\gamma\frac{\left\langle \frac{1}{R^3}\mathcal{H}(s)\right\rangle}{J_x\left\langle \frac{1}{R^2}\right\rangle}, \tag{18}$$

where,

$$\mathcal{H}(s) = \frac{\eta^2 + (\beta * \eta' + \alpha\eta)^2}{\beta}. \tag{19}$$

There are two things to notice about equations 18 and 19. First, in the limit that $R \to \infty$, the emittance $\epsilon_x \to 0$. Thus without bends the emittance floor is set by the injected emittance. Second, notice that equation 19 goes to zero when η and its derivative η' (dispersion and its derivative) go to zero. This shows that a wiggler in a dispersion free region has a purely damping effect. Ultimately, this ideal case cannot be met and in general the equilibrium emittance reached by a damping ring is dependent on the size of β in the wigglers.

The goals when optimizing a storage ring for low emittance are,

1. Obtain zero dispersion in the wigglers.

2. Minimize the impact of dispersion in the bends.

3. Lower β as much as possible in the wigglers.

By designing the storage ring correctly, the wiggler regions can be made completely dispersion free. Item 2 is then accomplished by increasing the tune of the machine. This is done by increasing the strength of the quadrupole magnets. The goal then becomes item 3, lowering β in the wigglers. To first order, the equilibrium emittance of the storage ring will be directly proportional to the size of β in the wigglers.

D. Chromaticity and Tune Spread

The force exerted on a particle in a magnetic field is proportional to the velocity of the particle. Therefore, particles with a momentum deviation will experience slightly stronger or weaker focusing, depending on whether the particle has a higher or lower momentum. Stronger focusing increases the tune of the lattice. Therefore, particles with a momentum deviation have a different tune. The amount by which the tune of a particle changes with momentum deviation is a property of the lattice and is given by,

$$\delta Q = \xi(p)\frac{\delta p}{p_0}, \tag{20}$$

where δQ is the change in tune, $\delta p/p$ is the energy spread, and ξ is the chromaticity. Typically, δQ is quite large and must be corrected with sextupole magnets.

Recalling equation 17,

$$x_g(s) = x(s) + D(s)\frac{\delta p}{p}, \tag{21}$$

we see that in dispersive regions the particles are displaced in the horizontal plane according to their momentum deviation. From equation 7 we can see that the sextupole term scales with x^2. We can therefore use sextupoles in dispersive regions to provide extra focusing for off-momentum particles. Particles with $\delta p/p = 0$ are follow a path along $x = 0$ and receive no extra focusing, while particles with $\delta p/p \neq 0$ follow a path along $x \propto \delta p/p$ and receive extra focusing proportional to their momentum deviation.

Using only two sextupoles, one for each transverse dimension, it is possible to set the chromaticity of a machine to zero. But usually this is not a good idea because it ruins the dynamic aperture of the machine. If the strength of a sextupole is too large, off-momentum particles will be strongly deflected and steered into the beam pipe. Strong sextupoles also couple the beam dimensions and excite higher order resonances. Chromaticity is best adjusted by using a large number of weak sextupoles, typically one per quadrupole.

The dynamic aperture of an accelerator can be thought of as a volume in phase space enclosing the particles that the accelerator is able to hold on to. Particles outside the dynamic aperture are lost by striking the beam pipe. This can happen if the particles are on a resonance that causes their betatron oscillations to grow. It can also happen if their injected phase-space displacement is outside the physical aperture of the machine.

Since the damped emittance of a storage is often a few orders of magnitude lower than the injected emittance, there are two considerations to take into account when judging

the dynamic aperture of a machine. First, the dynamic aperture must be large enough to facilitate injection. Having a dynamic aperture larger than 3-sigma of the injected emittance is usually sufficient. Dynamic apertures less than 3-sigma make injection difficult since a large proportion of particles will strike the beam pipe and be lost before damping can take effect. Second, once the particles are damped, the storage ring must hold on to them long enough to do something useful with them. This usually requires that the dynamic aperture be at least 10-sigma of the damped emittance.

In an ideal storage ring, there is one sextupole following each quadrupole. Tuning the chromaticity of the machine consists of adjusting these sextupoles to set the chromaticity to zero while maintaining the best possible dynamic aperture. As a rule of thumb, a lattice with a lower average sextupole moment will have a better dynamic aperture. In reality, coupling, different combinations of lattice functions, and nonlinearities come into play and sextupole optimization becomes a computational task.

E. Tune Footprints and Frequency Maps

As a particle makes it way around a storage ring, it undergoes betatron oscillations. The number of full oscillations it makes per loop is the integer tune of the machine. The actual tune of a particle has a fractional part. This fractional part determines the phase advance per revolution.

It is important to design the accelerator such that the fractional part of the tune causes misalignments in the lattice to cancel out over several revolutions. Imagine a magnet misaligned slightly so that it gives passing particles a very small kick when they pass through. If the fractional tune of a particle were such that the particle was at the exact same moment in its betatron oscillation every time it passes the misalignment, then the effect of the kicks will build up, resulting in excessive betatron oscillations and loss of the particle. On the other hand, if the fractional tune is set right, such that the particle encounters the kick at a different point in its betatron oscillation every time it passes by, the net effect will be that the kicks will cancel out over time and the effect of the misalignment negated.

The condition for resonances in the transverse plane is,

$$M \times Q_x \pm N \times Q_y = k, \tag{22}$$

where M, N, and k are integers. The $+$ sign gives sum resonances, while the $-$ sign gives difference resonances. Both sum and difference resonances couple the horizontal and vertical betatron motion of the beam. Difference resonances allow the amplitude of the beam to grow without bound, while with sum resonances, the sum of the squares of the amplitude of the betatron oscillations is bounded.

The order of the resonance is $P = |M| + |N|$. Lower order resonances are usually stronger, but easier to avoid since there are fewer of them. It is important to tune a storage ring so that the beam does not lay on any significant resonances, typically defined at those where P is less than 5 or 7. A tune plane with resonances up to $5th$ order is shown in figure 5.

A storage ring's position on the tune plane is determined by the strength of its quadrupoles. But recalling equation 20, the momentum deviation of a particle affects its tune. So the chromaticity of a storage ring, along with the equilibrium momentum spread of its particles, defines a footprint in the tune plane. Additionally, nonlinear elements, such as quadrupoles and wigglers, add a transverse displacement dependence to the tune. This

FIG. 5: Tune plane showing resonances up to third order. The fractional part of the tune must be positioned so as to not intersect these lines. Additionally, the tune footprint must be small enough such that particles do not spill over onto a resonance.

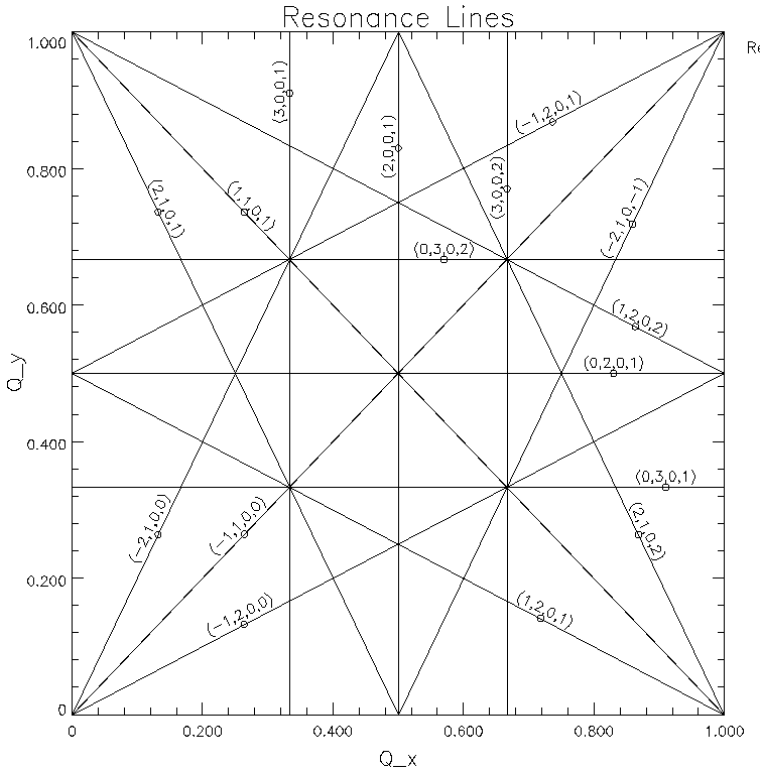

makes the tune of a particle dependent on the amplitude of its betatron oscillations. A realistic scenario is depicted in figure 6.

Figure 6 is a frequency map. It is produced in simulation by injecting a distribution of particles with a range of emittances and tracking them for about 1000 turns. A fast Fourier transform is then used to find the fractional tune of each particle for the first and last half of the turns. The particles are plotted on the tune plane according to their tune for the first half, and their color indicates how much their tune has changed by the second half. Particles that move around less on the tune plane (darker colors) are more stable. A frequency map provides us with information on how resonances are affecting the stability of the particles. Some resonances in figure 6 have a stronger impact on the frequency map than others. The quadrupoles can be used to move the footprint off more troubling resonances, and a well-optimized sextupole distribution will minimize the size of the footprint and the strength of the resonances.

F. Single and Multiple Event Coulomb Scattering

The effect of Coulomb scattering among the particles in the bunch becomes a significant in low emittance, high-intensity beams. The effect of the scattering is to couple the three bunch dimensions. In particular, we are interested in scattering events that transfer horizontal and vertical momentum to longitudinal momentum. Momentum transfered to the longitudinal dimension is boosted by relativistic effects, so through Coulomb scattering a small change

FIG. 6: Example of a realistic tune footprint. Plotted is the tune footprint of a CesrTA development lattice overlayed on a tune plane with resonances up to 7th order. The color of the dots is an indication of the stability of the lattice.

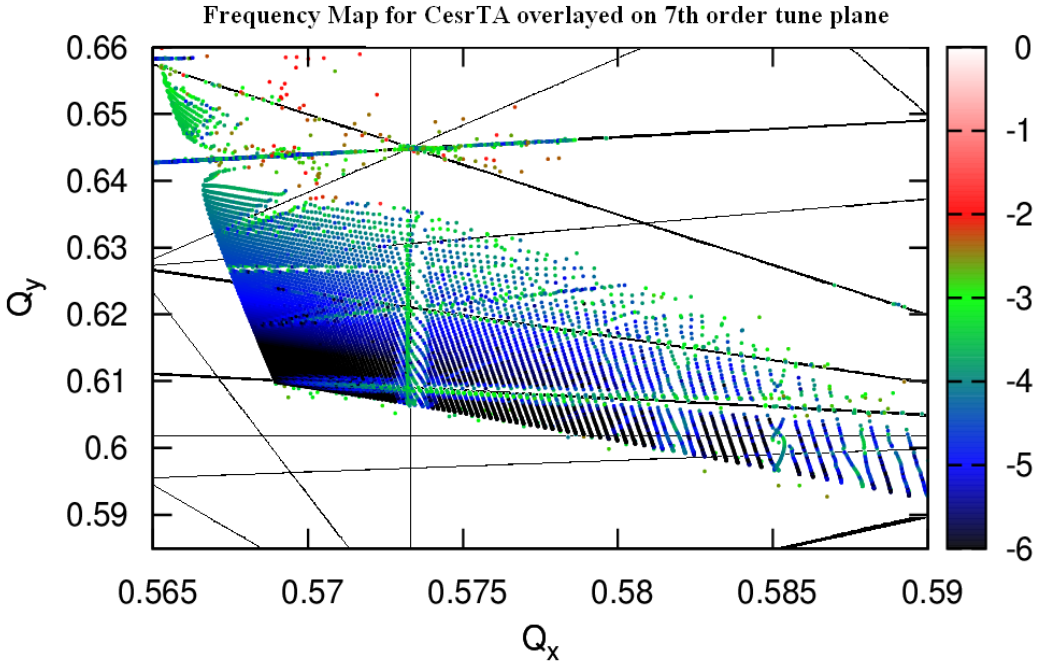

in transverse momentum results in a large change in longitudinal momentum.

A storage ring has a longitudinal momentum aperture commonly called the "RF bucket". The depth of the RF bucket is for the most part a function of the RF cavities. Particles with longitudinal momentum deviations that exceed this aperture are lost. If a collision between two particles transfers enough momentum to the longitudinal dimension, both particles are lost, one with too much momentum, and one with too little. Particle losses through this mechanism are called Touschek losses. The Touschek effect defines a beam lifetime that is significant in storage rings using intense, low emittance beams.

If the transfer of momentum is not enough to kick the particles out of the RF bucket, the particles are not lost, but their emittance is increased. Recalling equation 17, a momentum deviation will change the closed orbit of a particle. The same mechanism that allows photon emission in dispersive regions to increase the emittance of the beam, allows successive small momentum Coulomb scatterings to increase the emittance of the beam. Collisions change the momentum deviation of the particle, which shifts the particle's closed orbit, and the particle starts undergoing betatron oscillations around this new shifted orbit. This effect is called intrabeam scattering (IBS). Like the Touschek effect, IBS becomes significant in high particle density storage rings.

Since IBS depends on the rate of Coulomb scattering within the bunch, it depends on the density of the bunch. According to equation 17, in dispersive regions of the lattice the beam dimensions are blown up, and thus the density of the beam is reduced. This reduction in density decreases the frequency of collisions. On the other hand, dispersion is the mechanism through which IBS can increase the emittance of the bunch. The condition for minimizing

the effects of IBS is

$$T = \frac{\sigma_\beta^2}{\sigma_\beta^2 + \sigma_\eta^2} = 0.5, \tag{23}$$

where σ_β^2 is the beam size contribution due to emittance and σ_η^2 is the contribution due to dispersion.

Loosely said, for a given layout, the integrated amount of dispersion in a storage ring is conserved. That is, adjusting quadrupoles can only shift dispersion around from one place to another. Taking these considerations into account tells us that a storage ring designed to minimize the effects of IBS would consist two types of regions. One type where the dispersion is zero, and one type where dispersion accounts for half the beam size.

Shaping the dispersion function to minimize the effects of IBS isn't always possible. Its shape is also forced by the location of the wigglers, RF cavities, and instrumentation. In high beam density storage rings designed from the ground up, the needs of IBS, wigglers, and instrumentation can often all be met. But when reconfiguring a storage ring, such as we are doing with CESR, the requirements of wigglers and instrumentation leave little room for minimizing IBS effects.

III. DESIGNING AND OPTIMIZING THE CESR TEST ACCELERATOR

The CESR Test Accelerator will be built from the current CESR configuration by relocating 6 wigglers from the arcs to straight sections that can be configured for zero dispersion. A low dispersion region is created at the South interaction point for instrumentation. The strength of the quadrupoles is increased to increase the horizontal tune from 10 to 14, which reduces the emittance generated in the bends.

A. Low Emittance Tuning

With the wigglers positioned in dispersion free regions of the lattice, low emittance tuning consists of lowering the value of beta in the wigglers. The lowest obtainable emittance is given by theory as $\epsilon_h = 1.22$ nm [2]. The values of the beta function around a lattice are determined by the quadrupoles. The quadrupoles also determine the lattice's tune and dispersion function. The goal of low emittance tuning in a wiggler dominated storage ring is to lower beta in the wigglers while keeping the tune footprint off of resonances and the dispersion zero in the wigglers. This is done computationally with a program called TAO (Tool for Accelerator Optics). TAO is an optimizer in which we define variables and constraints. The program is set up with lattice's quadrupole strengths as variables. As constraints we define emittance, tune, dispersion, and a few other parameters that help ensure the stability of the lattice.

TAO optimizes a lattice using a standard optimization routine such as Differential Evolution [3] or Levenburg-Marquardt [4]. These routines work by adjusting the variables and observing how the constraints are affected. Depending on the routine used, the wiggling may or may not be guided by derivatives. Variable combinations that result in better constraints are tracked by the program, and the optimizer works its way down to a minimum.

We assume that the lattice is perfectly flat at this stage of development. Without vertical bends, there is zero vertical dispersion throughout the lattice, which, in turn, means that there is zero vertical dispersion-generated emittance. Without dispersion generated

emittance, the floor of the vertical emittance is determined by quantum uncertainty in the direction of the photons emitted due to horizontal bends. This quantum emittance is several orders of magnitude lower than the emittance due to coupling and is ignored. The vertical emittance is then dominated by coupling from the horizontal emittance. Typical storage rings operate with $\epsilon_y/\epsilon_x \approx 1\%$, although values as low as 0.1% have been achieved [5]. The causes of coupling are imperfections in the lattice, sextupoles, and other non-linear elements. Because vertical emittance due to emittance coupling is expected to be significant, we must optimize the horizontal emittance.

We optimized a total of 10 lattices with energies at 1.5, 2.0, 2.5, and 5.0 GeV, and wiggler fields at 12, 19, and 21 kG. The emittances achieved by the optimizer are shown in table II.

TABLE II: Lowest natural horizontal emittances achieved.

Energy (GeV)	Wiggler Field (kG)	Wiggler Count	Natural Horizontal Emittance (nm)
1.5	14	12	1.2
1.5	19	12	1.3
1.5	21	12	1.4
2.0	14	12	2.1
2.0	19	12	1.8
2.0	21	12	1.8
2.5	21	12	3.2
5.0	14	6	33.
5.0	19	6	28.
5.0	21	6	26.

B. Intrabeam Scattering

There are two principle methods for calculating IBS rates. A. Piwinski published a method in 1974 that is generally regarded to give results that agree fairly well with experimental data [6] . In 1983 J. Bjorken and S. Mtingwa published an improved method employing the scattering matrix formalism developed for quantum electrodynamics [7].

In a previous paper, I implemented in BMAD a number of methods for calculating a lattice's IBS properties. BMAD is the accelerator simulation package used at Cornell for the development and maintenance of CESR. I evaluated the Piwinski and Bjorken-Mtingwa methods, as well as numerous approximate methods, and concluded that the Completely Integrated Modified Piwinski method (CIMP) gave the best accuracy while still being quick to evaluate [8].

The equations used for evaluating IBS with CIMP are complicated and involve quantities that have not been discussed in this paper. Here we will simply state some of the more dominant relations that apply to high intensity electron storage rings. For more information on calculating IBS effects, see references [9] or [8].

Since vertical dispersion is small, the direct contribution to the vertical emittance from IBS will be small. We assume hereafter that the vertical IBS growth will be dominated by emittance coupling from the horizontal dimension.

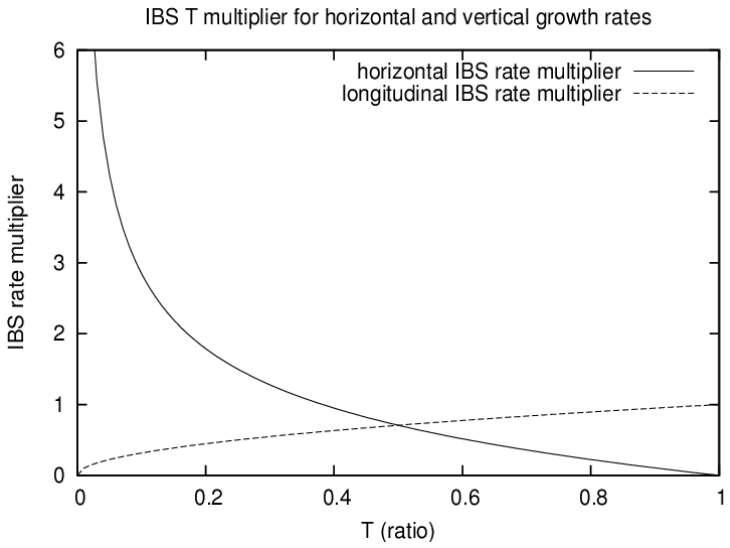

FIG. 7: Dependence of horizontal and longitudinal IBS growth rates on T-factor.

The T-ratio was introduced in equation 23. There we stated that the optimal value to minimize IBS effects was $T = .5$. The actual dependence of the IBS growth rates on T is,

$$\frac{1}{\tau_H} = \frac{(1-T)}{\sqrt{T}} * G(lattice functions), \tag{24}$$

$$\frac{1}{\tau_P} = \sqrt{T} * G(lattice functions), \tag{25}$$

where $\frac{1}{\tau_H}$ is the horizontal growth rate and $\frac{1}{\tau_P}$ is the longitudinal growth rate. A plot of equations 24 and 25 is shown in figure 7.

We see that for $T \to 0$, where the beam size is dominated by dispersion, the longitudinal growth rate goes to zero, while the horizontal rate blows up as $1/\sqrt{T}$. As $T \to 1$, the horizontal rate goes to zero while the longitudinal multiplier goes to 1. The curves intersect at .5.

We find that for CesrTA the majority of the lattice has a low T value. A histogram of the CesrTA lattice is shown in figure 8. The low value of T tells us to expect that IBS blow effects will be significant in CesrTA. Attempts to reshape the dispersion function to shift T to higher values were hindered by the necessity to keep dispersion zero in the wigglers and RF cavities.

IBS scales with γ and particles per bunch N as

$$\frac{1}{T_{h,v,p}} \propto \frac{N}{\gamma^4}. \tag{26}$$

According to equation 26, we can probe IBS effects by changing beam energy and N. Figure 11 shows the effect of increasing the beam energy from 2.0 GeV to 2.5 GeV. Since IBS rates vary directly with particles per bunch, we typically plot IBS effects as a function of N. The bunch charge specified for the ILC is $N = 2 \times 10^{10}$ particles per bunch. We explore in CesrTA bunch charges ranging from 0 to 2×10^{10}.

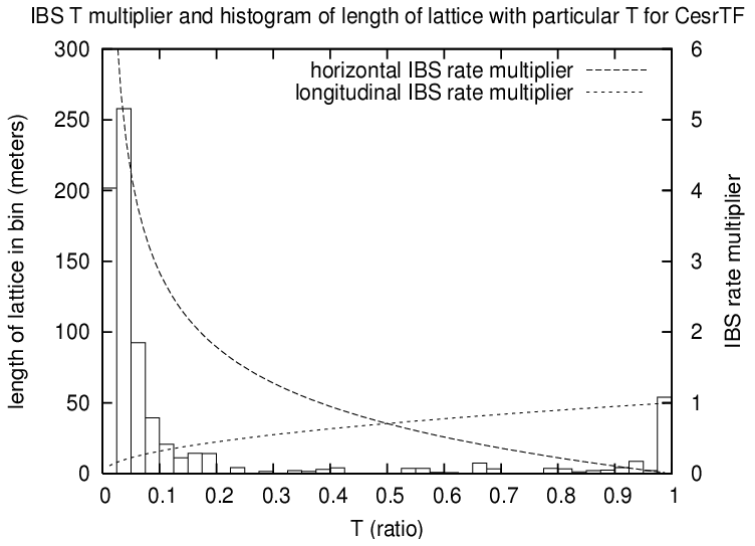

FIG. 8: Histogram of length of CesrTA track binned by T ratio.

The equilibrium emittance with IBS included occurs when the IBS growth rates are balanced by radiation damping,

$$(\frac{d\epsilon_{h,v,p}}{dt})_{IBS} = (\frac{d\epsilon_{h,v,p}}{dt})_{SR}. \tag{27}$$

We define the IBS growth time as $T_{h,v,p}$ and the SR damping time is $\tau_{h,v,p}$. Note that while $\tau_{h,v,p}$ is constant, $T_{h,v,p} = T_{h,v,p}(\epsilon_h, \epsilon_v, \epsilon_p)$; we will refer to it simply at $T_{h,v,p}$. The rates are defined as,

$$(\frac{d\epsilon_{h,v,p}}{dt})_{SR} = 2\frac{\epsilon_{h,v,p} - \epsilon_{h0,v0,p0}}{\tau_{h,v,p}}, \tag{28}$$

$$(\frac{d\epsilon_{h,v,p}}{dt})_{IBS} = 2\frac{\epsilon_{h,v,p}}{T_{h,v,p}}, \tag{29}$$

where $\epsilon_{h0,v0,p0}$ refers to the emittance due to quantum excitation and synchrotron radiation alone. The factors of 2 arise because, by convention, IBS and SR rates are given as betatron rates; the factor of two converts them to emittance rates.

Substituting equations 28 and 29 into equation 27 and solving for ϵ yields

$$\epsilon_{h,v,p} = \frac{T_{h,v,p}}{T_{h,v,p} - \tau_{h,v,p}}\epsilon_{h0,v0,p0}. \tag{30}$$

Equation 30 is our basic equation for calculating equilibrium, but it does not yet take into account that the natural vertical emittance has both a coupling part and a dispersion part, $\epsilon_{v0} = \epsilon_{v0,\eta} + \epsilon_{v0,\kappa}$. While the dispersion part is constant, the coupling part depends on the horizontal emittance. We define $r_e = \epsilon_{v0,\kappa}/\epsilon_{v0}$ and rewrite equation 27 for the vertical dimension as

$$\epsilon_v = [(1 - r_e)\frac{T_v}{T_v - \tau_v} + r_e\frac{T_h}{T_h - \tau_h}]\epsilon_{v0}. \tag{31}$$

Studies on our ability to correct for magnet misalignments leads us to expect that we can operate CesrTA with zero current emittances of 3-8 pm at 2.0 GeV [10]. In order to

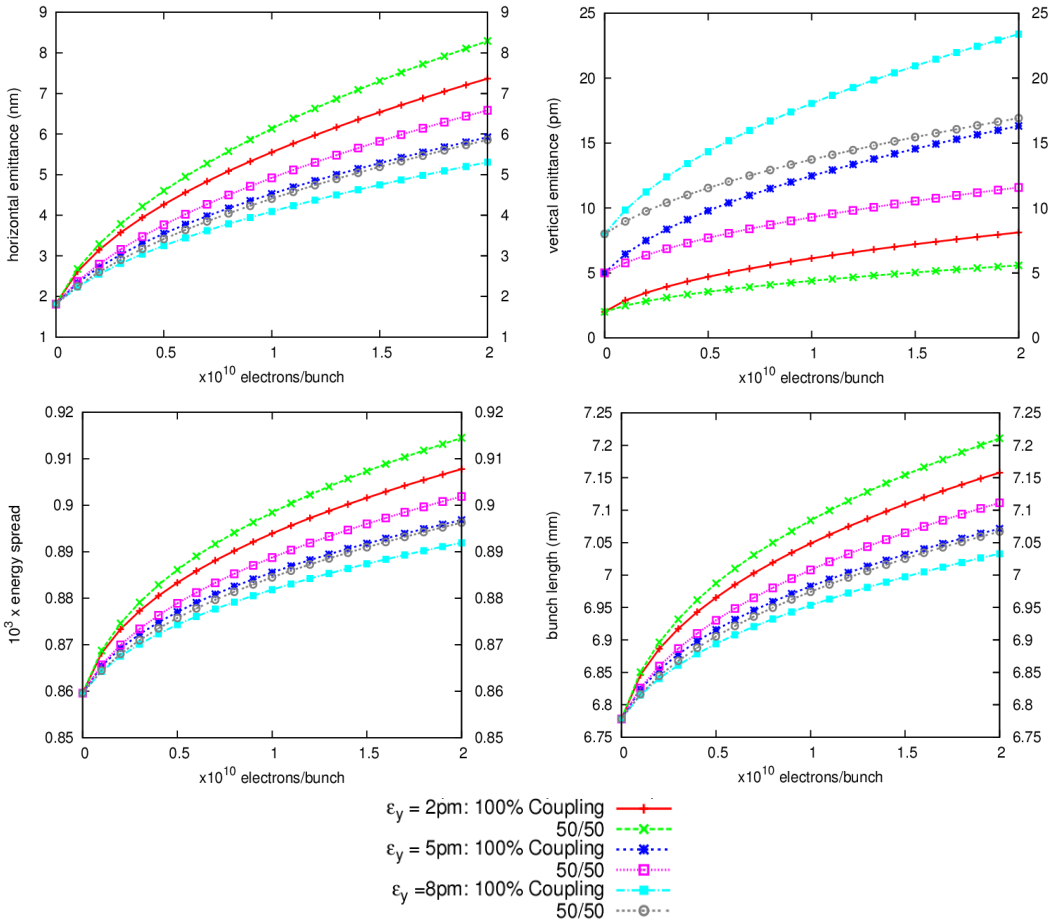

FIG. 9: Equilibrium beam parameters for CesrTA at 2.0 GeV with twelve 21 kG wigglers from zero current up to the ILC bunch charge, 2×10^{10}.

evaluate the range of IBS growth rates that can be expected, we explicitly consider the two cases: $r_e = 1$ where the vertical emittance growth is entirely due to emittance coupling, and $r_e = 0.5$ where the vertical emittance growth is due both to emittance coupling and vertical dispersion. For each case we consider 3 possible zero current emittances: 2, 5, and 8 pm. Figure 9 shows the results for CesrTA at 2.0 GeV with twelve 21 kG wigglers. For this lattice we expect IBS effects to blow up the horizontal beam emittance by a factor of 3 to 4 and the vertical emittance by a factor of about 2 to 3.

The 2.5 GeV lattice was produced to explore the effect of increasing beam energy on IBS effects. Recall that IBS rates have a $1/\gamma^4$ dependence. The results are shown in figure 10. We find that increasing the beam energy from 2.0 GeV to 2.5 GeV increases the natural emittance, but decreases IBS to the extent that the equilibrium is significantly lower. The vertical emittances for the 2.0 GeV case and 2.5 GeV case are compared in figure 11.

Table III is summary of the results of IBS calculations on all ten CesrTA lattices at high current.

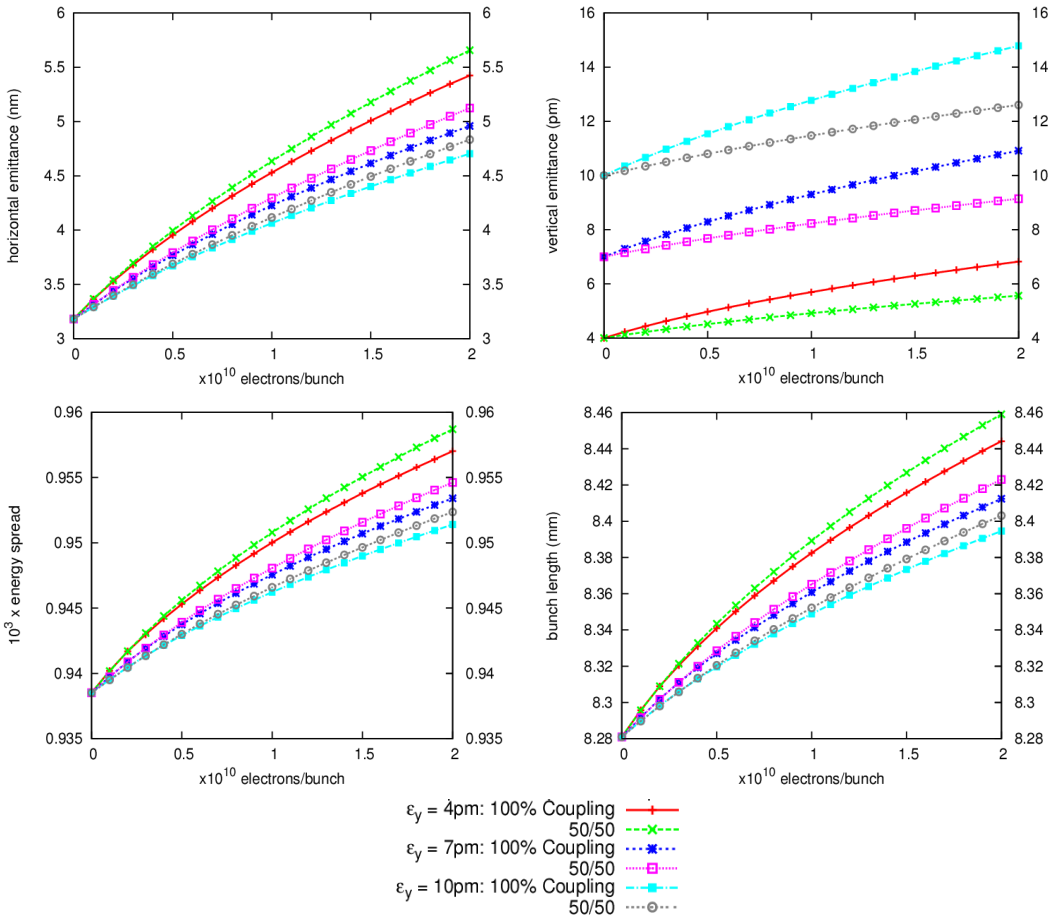

FIG. 10: Equilibrium beam parameters for CesrTA at 2.5 GeV with twelve 21 kG wigglers,from zero current up to the ILC bunch charge, 2×10^{10}.

C. Touschek Effect

The Touschek effect is closely related to the IBS effect. In cases where the momentum transfer due to a Coulomb scatter is large, both particles are lost, one with too much momentum and with too little. The Touschek effect is different in that instead of integrating over collisions to determine a rise-time, we integrate over the number of collisions that result in a longitudinal momentum transfer that exceeds a predetermined cutoff.

The cutoff is determined by two different momentum apertures. The first aperture is the depth of the RF-bucket defined by

$$\left(\frac{\delta E}{E}\right)^2 = \frac{U_0}{\pi|\eta|hE_0}F(q), \tag{32}$$

and

$$F(q) = 2\left[\sqrt{q^2-1} - cos^{-1}(1/q)\right], \tag{33}$$

where $q = e \times V_{rf}/U_0$ and $U_0 = \frac{(8.84\times10^{-5})}{2\pi}E^4\mathcal{I}_2^4$. $\delta E/E$ is the acceptable momentum deviation. Particles with momentum deviation that exceed the RF bucket depth are lost

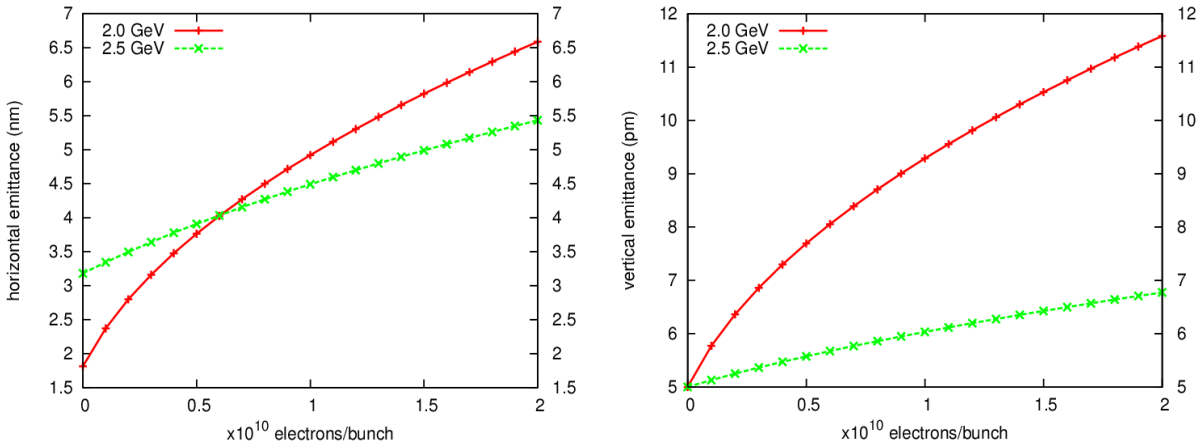

FIG. 11: Comparison of effect of IBS on CesrTA at 2.0 GeV and 2.5 GeV. Notice that while increasing the energy increases the natural emittance, it also mitigates the IBS effects, resulting in a lower emittance at high currents. At both energies, $\epsilon_{y0} = 5$ pm and $r_e = 0.5$ were assumed.

longitudinally. The second is due to the dynamic aperture of the machine. The dynamic aperture of CesrTA will be discussed in detail in the next section. For now it is sufficient to know that particles with too large a momentum deviation will have large betatron oscillations and hit the beam pipe. Such particles are lost transversely. The maximum $\delta E/E$ calculated for each effect for each lattice is in table IV. The smallest aperture of these two effects is used in the Touschek calculations.

The Touschek lifetime is a half-life; it is defined as the amount of time it takes for half of the particles in a bunch to be lost. The rate of particle loss is linear in particles per bunch. This allows us to define a parameter

$$a = \frac{1/T_l}{N_0}, \tag{34}$$

where N_0 is the initial number of particles per bunch, and $1/T_l$ is the Touschek lifetime given by equations (41) and (42) from reference [11]. We can then write an equation for how the number of particles in the bunch changes over time,

$$N(t) = \frac{N_0}{1 + N_0 a t}. \tag{35}$$

Both the Touschek effect and IBS effect are dependent on the dimensions of the bunch and the number of particles in the bunch. While the Touschek effect changes over time the number of particles in the bunch, the IBS effect changes over time the dimensions of the bunch. It is therefore necessary when examining the Touschek effect to evolve the beam step-wise through time, reevaluating the beam size and loss rate after each step.

We assume that a natural vertical emittance of $\epsilon_{y0} = 5.0$ pm, a dispersion ratio of $r_e = .5$, and 2.0×10^{10} initial particles per bunch. Table IV contains the initial and evolved bunch half-life. The evolved half-life comes from a stepwise evolution of the beam through time. In figure 12 the number of particles per bunch and vertical emittance are plotted versus time for the baseline 2.0 GeV CesrTA lattice with 12 wigglers operating at a peak field of 21 kG.

TABLE III: Equilibrium emittance after IBS effects at high current (N = 2×10^{10} particles/bunch). For the 1.5 GeV lattices, the range represents r_e at 0.3 and 0.8. For the 2.0 and 2.5 GeV, the range represents r_e at 0.5 and 1.0. For 5.0 GeV, we assume the vertical emittance will be completely dominated by coupling, $r_e = 1.0$

Energy (GeV)	Wiggler Field (kG)	Wiggler Count	Zero Cur. Horizontal Emittance (nm)	Zero Cur. Vertical Emittance (pm)	High Cur. Horizontal Emittance (nm)	High Cur. Vertical Emittance (pm)	High Cur. Bunch Length (mm)	RF Voltage (MV)
1.5	14	12	1.2	2.0	18. - 22.	12. - 23.	7.5 - 7.8	7.0
				5.0	14. - 17.	25. - 47.	7.2 - 7.5	10.
				8.0	13. - 16.	35. - 66.	7.1 - 7.3	11.
1.5	19	12	1.3	2.0	14. - 17.	9.4 - 18.	6.9 - 7.0	11.
				5.0	11. - 13.	19. - 35.	6.7 - 6.9	15.
				8.0	9.6 - 12.	27. - 50.	6.6 - 6.8	15.
1.5	21	12	1.4	2.0	13. - 16.	8.1 - 15.	6.8 - 6.9	15.
				5.0	10. - 12.	17. - 30.	6.6 - 6.7	15.
				8.0	9.0 - 11.	24. - 42.	6.5 - 6.7	15.
2.0	14	12	2.1	2.0	12. - 13.	7.3 - 11.	6.9 - 7.0	15.
				5.0	9.3 - 10.	15. - 22.	6.7 - 6.8	15.
				8.0	8.3 - 9.3	22. - 32.	6.6 - 6.7	15.
2.0	19	12	1.8	2.0	8.2 - 9.2	6.1 - 9.0	6.9 - 6.9	15.
				5.0	6.6 - 7.3	13. - 18.	6.8 - 6.8	15.
				8.0	5.9 - 6.5	18. - 26.	6.7 - 6.8	15.
2.0	21	12	1.8	2.0	7.4 - 8.3	5.6 - 8.1	7.2 - 7.2	15.
				5.0	5.9 - 6.6	12. - 16.	7.1 - 7.1	15.
				8.0	5.3 - 5.9	17. - 24.	7.0 - 7.1	15.
2.5	21	12	3.2	4.0	5.4 - 5.7	5.6 - 6.8	8.4 - 8.5	15.
				7.0	5.0 - 5.1	9.1 - 11.	8.4 - 8.4	15.
				10.	4.7 - 4.8	13. - 15.	8.4 - 8.4	15.
5.0	14	6	33.	66.	33.	66.	9.3	15.
				99.	33.	99.	9.3	15.
5.0	19	6	28.	56.	28.	56.	12.	15.
				84.	28.	84.	12.	15.
5.0	14	6	26.	52.	26.	52.	13.	15.
				78.	26.	78.	13.	15.

D. Sextupole Optimization

Recalling equation 20, the tune of a particle depends on its momentum deviation according to

$$\delta Q = \xi(p)\frac{\delta p}{p_0}, \tag{36}$$

where ξ is the chromaticity. The natural (uncorrected) chromaticity of CesrTA is a consistent -22 in the horizontal and -17 in the vertical across all 10 lattices. In order to minimize the size

TABLE IV: Touschek lifetime of CesrTA lattices.

Energy (GeV)	Wiggler Field (kG)	Wiggler Count	RF Bucket $\delta E/E$ (%)	Dynamic Aperture $\delta E/E$ (%)	Initial Touschek half-life (minutes)	Evolved Touschek half-life (minutes)
1.5	14	12	1.2	1.0	33.6	30
1.5	19	12	1.5	1.0	25.1	22
1.5	21	12	1.6	1.0	22.1	20
2.0	14	12	1.8	1.5	103.7	92
2.0	19	12	1.8	1.5	90.8	82
2.0	21	12	1.8	1.5	88.9	80
2.5	21	12	1.6	1.5	139.0	130
5.0	14	6	1.0	2.5	523.8	524
5.0	19	6	1.0	2.5	620.0	620
5.0	21	6	1.0	2.5	666.7	668

of the tune footprint, the chromaticity must be corrected to near zero in both dimensions. Sextupole magnets are used to correct the chromaticity to 1.0. We use 1.0 instead of zero because multi-bunch effects create a chromaticity spread in the machine, and it is important to ensure that none of the bunches in the accelerator have a negative chromaticity. Negative chromaticities can cause the head-tail instability. The head-tail instability is a process where wake fields excited by the front of the bunch induce transverse motion of the tail leading to rapid growth in the bunch size.

The criteria for a good sextupole distribution is that it set the chromaticity to the desired value without destroying the dynamic aperture of the machine. The effect a sextupole distribution will have on the dynamic aperture can be predicted by looking at the nonlinearities it causes in the storage ring. The nonlinearities we look at are the derivative of beta with respect to energy ($d\beta(s)/dE$) and the determinant of the transfer matrix of the ring.

Setting a bound on the amplitude of $d\beta(s)/dE$ ensures that no one segment of the lattice looks too different for off-energy particles. Recall that the chromaticity is a global quantity

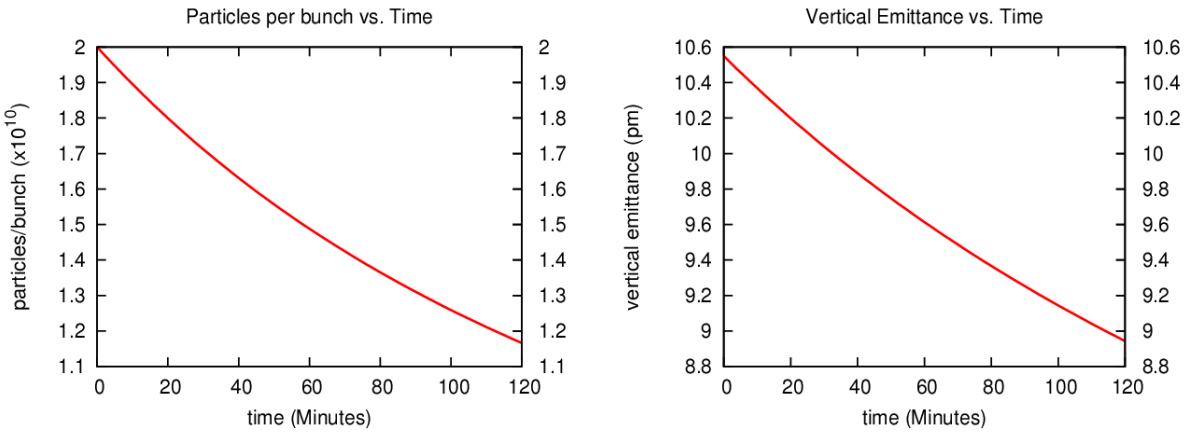

FIG. 12: Particles per bunch and vertical emittance versus time for CesrTA at 2.0 GeV with twelve 21 kG wigglers.

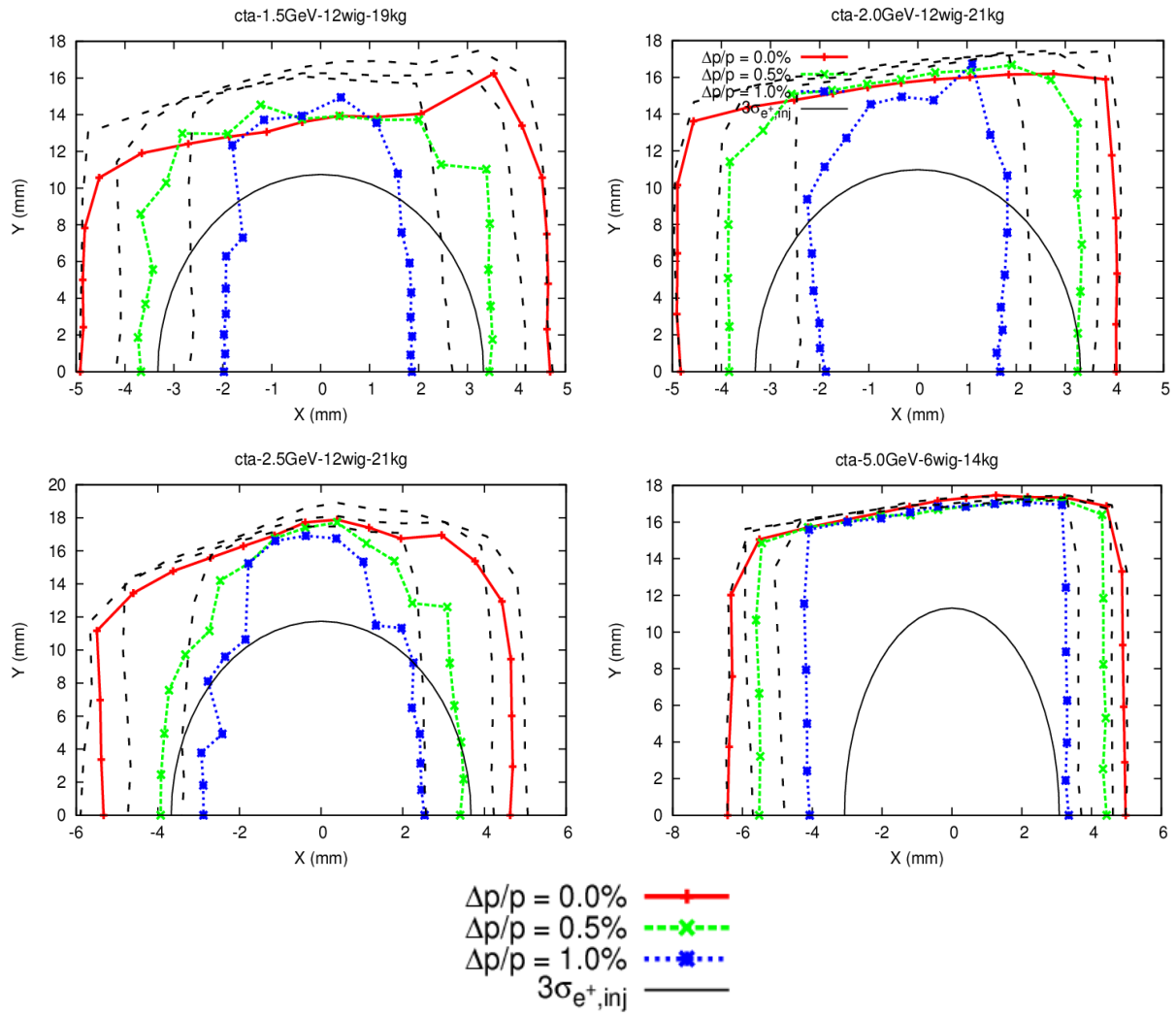

FIG. 13: Representative dynamic apertures for each CesrTA energy. The dotted lines represent the physical aperture and are just larger than the dynamic aperture curves they correspond to. The solid black curve is 3-sigma of the injected emittance. Three energy offsets are examined, 0.0%, 0.5%, and 1.0%.

characterizing the lattice defined by $\delta Q = \xi \times \delta p/p$, where ξ is the chromaticity and depends on the variation of the beta functions with energy. In general, the dynamic aperture of the ring will be maximized when the variations of the beta functions with energy are minimized.

A storage ring is a sequence of optical elements. Each element can be described by a transfer matrix and the transfer matrix of the ring is given by the product of all the individual transfer matrices. The determinant of the transfer matrix of the ring in a perfectly linear machine is 1 and does not change with deviations from the ideal orbit. The determinant in a nonlinear machine will deviate from 1 as you travel away from the ideal orbit. Imposing a constraint that the determinant of the transfer matrix of the ring not deviate from one as you travel away from the ideal orbit helps to ensure that the sextupole distribution introduces as few nonlinearities as possible.

The process for optimizing the sextupole distribution is similar to that for optimizing the quadrupole distribution. It is done computationally with BMADZ, a program similar to TAO. We define as variables the sextupole strengths, and as constraints, the chromaticity, amplitude of $d\beta(s)/dE$, and the determinant of the transfer matrix of the ring. The optimizer computes numerical derivatives of the constraints with respect to the variables. It uses these derivatives to adjust the variables such that the constraints are minimized. Through this optimization process it is possible to generate sextupole distributions that optimize the dynamic aperture of the machine.

TABLE V: Chromaticity and Dynamic Aperture Properties of CesrTA. The data here is for a lattice with chromaticity set to approximately 1 in x and y.

Energy (GeV)	Wiggler Field (kG)	Wiggler Count	Dynamic Aperture at 0.0% energy spread (stored beam sigma)	Dynamic Aperture at 1.0% energy spread (stored beam sigma)
1.5	14	12	9.3	3.2
1.5	19	12	10.0	3.9
1.5	21	12	9.1	3.8
2.0	14	12	11.5	6.7
2.0	19	12	10.4	5.4
2.0	21	12	10.7	4.3
2.5	21	12	12.3	5.2
5.0	14	6	15.2	10.1
5.0	19	6	14.0	8.0
5.0	21	6	14.4	9.5

The dynamic aperture of a design is determined by tracking particles having a range of initial position, angle, and energy deviations from the ideal orbit. The range of these initial parameters for which the particle motion remains stable determines the dynamic aperture of the lattice. The distribution is in phase space, and a closed path can be drawn between the particles that survive and those that are lost. The area enclosed by this path is the dynamic aperture. It is typically given in units of sigma of the injected emittance. For example, a storage ring with a 3-sigma dynamic aperture can hold on to a particle distribution 3 times larger than the sigma of the particles injected into it.

Selected dynamic aperture plots are in figure 13. The dynamic apertures for all ten CesrTA lattices in units of injected emittance are shown in table V.

IV. CONCLUSION

The parameter space for CESR as an ILC damping ring test facility has been characterized. We find that the facility has the potential to generate electron and positron beams with vertical emittances less than 10 pm. The lifetime after IBS and Touschek effects are taken into account is quite long, ranging from 30 minutes to long as several hours. We also find that the dimensions and charge of the bunches will be reasonably constant over that period of time.

We find that intrabeam scattering will be a significant effect in CesrTA. Using handles such as beam energy, bunch charge, and the ability to produce both electron and positron

beams, we can disentangle IBS from other effects of interest. CesrTA will therefore be useful for exploring the properties of IBS and other low emittance effects, such as ion instabilities. The dynamic aperture of CesrTA will be large enough that injection should not be a problem.

The types of beams CesrTA will be able to generate and their long lifetimes will enable us to test accelerator technologies for use in the ILC damping rings. Examples include modified beam pipes that allow the concentration of free electron gas in the pipe to be measured, and wigglers and SRF cavities.

---

[1] ILC Global Design Effort. "ILC Reference Design Report 2007", available at: http://media.linearcollider.org/report-apr03-part1.pdf

[2] M. Palmer. "Emittance Reach for Operating CESR as a Damping Ring Test Facility", available at: https://wiki.lepp.cornell.edu/ilc/pub/Public/CesrTA/WebHome/emittance_memo.pdf

[3] R. Storn and K. Price., "Differential Evolution - a Simple and Efficient Adaptive Scheme for Global Optimization over Continuous Spaces", Technical Report TR-95-012, ICSI, March 1995.

[4] K. Levenberg. "A Method for the Solution of Certain Problems in Least Squares." Quart. Appl. Math. 2, 164-168, 1994.

[5] C. Steier. *et al.* "Coupling Correction and Beam Dynamics at Ultralow Vertical Emittance in the ALS", Proceedings of the 2003 Particle Accelerator Conference.

[6] A. Piwinski. "Intra-Beam-Scattering", in *Proceedings of the 9th International Conference on High Energy Accelerators, Stanford, CA, 1974* (SLAC, Stanford, 1974), p. 405.

[7] J. D. Bjorken, S. K. Mtingwa. "Intrabeam Scattering", Part. Accel. **13**, p. 115, 1983.

[8] M. Ehrlichman. "Intrabeam scattering studies for the CESR damping ring test facility" available at: http://www.physics.umn.edu/ ehrlichman/ehrlichman-ibs.pdf

[9] K. Kubo. *et al.* "Intrabeam scattering formulas for high energy beams", Phys. Rev. ST Accel. Beams **8**, 081001 (2005).

[10] M. Palmer *et al.* "The Proposed Conversion of CESR to an ILC Damping Ring Test Facility", in *Proceedings of EPAC 2006, Edinburgh, Scotland*, p. 891.

[11] A. Piwinski. "The Touschek Effect in Strong Focusing Storage Rings" DESY 98-179